Mineralogical and Elemental Analysis of Hendrina Fly Ash

Alegbe, M.J[1], Moronkola, B.A[1], Omowonuola, A[1], O.O, Fatoba[2], P Ndungu[2] and Petrik, L.F[2]

[1]Chemistry Department, Lagos State University Ojo campus, Lagos Badagry expressway, Lagos, Nigeria

[2]Enviromental and NanoSciences Group, Chemistry Department, University of the Western Cape, Private Bag X17, Bellville 7535, South Africa.

ABSTRACT

Coal is the major source of electricity in South Africa and a large volume of coal fly ash waste is generated by the thermal fired power stations which have become a serious environmental issue because of the problem of the disposal. The aim of this research is to assess the quality and beneficiation of the coal fly ash samples. The fly ash sample was characterized using analytical techniques such as X-ray diffraction (XRD), X-ray fluorescence (XRF), scanning electron microscopy (SEM) and Fourier transform infrared (FTIR) spectroscopy. The morphology of the fly ash is spherical and the XRD identified mullite, gypsum, magnetite, lime, quartz and hematite mineral phases. The elemental composition of the fly ash using XRF containing major elements: SiO_2, Al_2O_3, Fe_2O_3, CaO, while the minor elements are P_2O_5, SO_3, MgO, NaO, TiO_2, and V_2O_5. The result shows that the coal fly ash sample is class C ash with high pozzolanic properties that is suitable to be used for making concrete or cement.

1.0 Introduction

Coal fly ash is a fine and powdery major solid product of thermal power plants that can cause pollution if discharged into the environment (XU *et al*., 2017). One of the major problems in most countries using coal to generated electricity from thermal power plant stations is the disposal of large amount of fly ash the water resource and environment. Coal-based electricity power plant is the major source of electricity in South Africa with the generation of coal fly ash wastes. The properties of the coal fly ash are different depending on the source, type of coal and the mode of operation of the power plant. The utilization of South African coal fly ash depends on the local need and the purpose for which the ash wastes is required to be used for (). In the building industry, fly ash can be used in concrete as a partial replacement of cement and/or sand to enhance the workability of fresh concrete, to reduce heat of hydration and to improve concrete permeability and resistance to sulphate attack (). The beneficiation of certain fly ash materials may be required, to either improve its properties to achieve homogeneity or for the specific use (). The commercial value and beneficial qualities of fly ash in concrete is based on its properties if it falls within certain limits of particle size classification and control of unburnt coal (Hower et al., 2017). The presence of unburned carbon in coal fly ash will decrease the compressive strength of the cement. First grade standard specification of coal fly ash limits the loss-on-ignition (LOI) values by less than 5% if the parameter provides good estimation of carbon content. However, the LOI of most China thermal power plants fly ash is in the range of 15%-20% (Huang et al., 2003; Asokan et al., 2005; Sahbaz et al., 2008; Lee, et al. 2010). The different residues generated from the combustion of coal are coal fly ash, flue gas, bottom ash, desulphurization waste, coal gasification and fluidized bed boiler waste. The disposal huge quantity of fly ash waste by thermal power stations huge problem because it will require large expanse of land (Parisara 2007).

The highest utilization was in cement industry (&49%), whereas, agricultural sector contributed very less (&1%). The FA is also generated by factory boilers, cement industry etc. which adds more to this quantity. The common practice to dispose huge quantity of FA is disposal at the dumping site, which requires huge quantities of land and causes deterioration of air, soil and water quality. Fly ash is mostly utilized as a soil amendment in agriculture, used to buffer the soil pH (Phung et al.1978), improving soil texture (Chang et al. 1977), improving nutrient status of the soil (Rautaray et al. 2003), etc. But most of the FA still remains in the ash pond, causing many deleterious effects on the environment, resulting in the degradation of land due to accelerated erosion rates. The use of biomass as a fuel is commonly used and it produces large quantity of residual ash which also causes serious environmental problems (Foo and Hameed 2009).

Coal combustion produces various types of residues such as fly ash, bottom ash, and flue gas desulphurization waste, fluidized bed boiler waste and coal gasification ash. The residues from coal combustion entering the flue gas stream are known as fly ash (FA). An energy sector of India accounts for nearly 13 million tons of FA generation per year. Fly ash production in year 2005–2006 in India was 112 million tons and is expected to reach about 170 million tons year-1 by the end of 2012 (MOEF 2007) (Table 1).The disposal of such a huge quantity of FA is a big problem in an area around the thermal power station. According to World Bank, India will require 1,000 sq. km. of land for the disposal of coal ash till 2015 (Parisara 2007). Therefore, there is the need of new and innovative methods for reducing the negative impacts of the FA on the environment. The formation of FA depends on the quality of the coal. In general, Indian coal produces relatively high amount of ash (10–30%) in comparison to other countries.

Tele:
E-mail address: alegbemj@gmail.com

In India, total annual generation of FA was 40 million tonnes during 1994, which had increased and reached about 112 million tonnes till March, 2005 and is estimated to reach up to 170 million tonnes by the year 2012 (Rajamane 2003). Whereas, the utilization of FA which was 3% of 40 MT production in 1994, has increased and reached about 38% (42 MT) of total production i.e., 112 MT during 2004–2005 which is far below the global utilization rate (Dhadse et al. 2008) (Table 1). In India, major portion of FA disposed into the ash ponds and landfills, very small percentile of FA (\15%) is being used for preparing bricks, ceramics and cements (Pandey et al. 2009). The total utilization of FA in 2004–2005 was about 42 Million tonnes per year. The highest utilization was in cement industry (&49%), whereas, agricultural sector contributed very less (&1%). The FA is also generated by factory boilers, cement industry etc. which adds more to this quantity. The common practice to dispose huge quantity of FA is disposal at the dumping site, which requires huge quantities of land and causes deterioration of air, soil and water quality. Fly ash is mostly utilized as a soil amendment in agriculture, used to buffer the soil pH (Phung et al.1978), improving soil texture (Chang et al. 1977), improving nutrient status of the soil (Rautaray et al. 2003), etc. But most of the FA still remains in the ash pond, causing many deleterious effects on the environment, resulting in the degradation of land due to accelerated erosion rates. The use of biomass as a fuel is commonly used and it produces large quantity of residual ash which also causes serious environmental problems (Foo and Hameed 2009). Like in the case of coal ash, biomass ash does not contain toxic metals. The ash forming constituents in biomass fuels are quite diverse depending on the type of biomass, type of soil and harvesting (Thy et al. 2006). The present review deals with the positive and negative aspect of fly ash utilization in agriculture. Review also put forth the heavy metal accumulation into the plant and its response by the application of fly ash into the soil. Reduction of negative effects of fly ash is important for its sustainable utilization in agriculture.

1.1 Physicochemical properties of fly ash

The physico-chemical properties of FA primarily depends on the parent coal composition of which it is produced and secondly on its coal combustion condition. Due to varying nature of coal the FA characteristics are also varies. The coal is a complex polymeric solid having no repeating monomeric units. Generally fly ash is grey in colour, abrasive, mostly alkaline, and refractory in nature (Ahmaruzzaman 2010). The chemical characteristics of coal are described by the parameters such as molecular weight, carbon aromaticity, normal aromatic and aliphatic structure and functional groups. The rank of coal is described by criteria like its vitrinite reflectance, oxygen content, calorific value, ultimate analysis, fixed carbon etc. (Speight 2005). Generally, Indian coals have a high mineral matter percentage, low sulphur content, high moisture, high ash content and low calorific value (3,500–4,000 kcal kg-1). Ash content of Indian coals varies between 15 to 30% and the S content is generally less than 1% (Srivastava 2003; Bhatt 2006). It is very hard to generalize the composition of ashes. Whereas, chemical composition of FA depends on the parent coal quality and its operating conditions (Jala and Goyal 2006). Fly ash consists of approximately 95–99% oxides of Si, Al, Fe and Ca and about 0.5 to 3.5% of Na, P, K and S and the remaining ash are trace elements (Kumar et al. 1998; Gatima et al. 2005). Typical FA constituents are SiO_2 (49–

67%), Al_2O_3 (16–29%), Fe_2O_3 (4–10%), CaO (1–4%), MgO (0.2–2%), SO_3 (0.1–2%) (Anon 2006). Certain characteristics of FAs are fairly uniform. Fly ash consists of much minute glass like particles of 0.01 to 100 mm size (Davison et al. 1974; Bhanarkar et al. 2008) having specific gravities 2.1 to 2.6 g m-3 (Bern 1976). Some spheres of FA are hollow (cenospheres), while others (plerospheres) are filled with small amorphous particles (Hodgson and Holliday 1966). Bulk density of FA ranges from 1 to 1.8 g cm3, whereas pH varies from 4.5 to 12.0 depending on parent coal S content (Plank and Martens 1974). The alkaline pH of FA may be due to the presence of Ca, Na, Mg and OH along with other trace metals. CaO, a major constituent of the FA, forms Ca (OH)2 with water and, thus, attributes towards alkalinity (Hodgson et al. 1982). The particle size of FA greatly influences its composition; however, it also affects the soil physical properties. All the metals present in soil are found in the FA. Comparative study of physico-chemical characteristics of FA and soil is given in Table 2. The concentration of various elements found in FA varies according to the particle size (Davison et al. 1974; Khan and Khan 1996). Some of the important elements constituting FA are Si, Ca, Mg, Na, K, Cd, Pb, Cu, Co, Fe, Mn, Mo, Ni, Zn, B, F and Al (Singh and Yunus 2000; Tripathi et al. 2004; Gupta and Sinha 2008; Jala and Goyal 2006; Ahmaruzzaman 2010) (Table 2). Therefore, FA contains all the important metals needed for plant growth and its metabolism except organic carbon and nitrogen (Jala and Goyal 2006). Fly ash contains very less or no nitrogen as the N present in the coal is volatilized during its combustion (Bradshaw and Chadwick 1980; Singh and Yunus 2000), however it has high concentration of phosphorous (P) (400–8,000 mg P kg-1), but the form of P is not readily available to plants, probably due to interactions with Al, Fe and Ca present in alkaline FA. Some important physicochemical characteristics of fly ash, such as bulk density, particle size, porosity, water holding capacity, and surface area render them suitable to be used as adsorbent (Ahmaruzzaman 2010). Presence of radionuclides inFAhas been reported by several workers but the literature on their impact has been less (Coles et al. 1978; Gowiak and Pacynas 1980; Mittra et al. 2005). Mittra et al. (2005) in a study analyzed the radioactivity (Bq kg-1) of fly ash and reported higher radioactivity of 226Ra, 228Ac and 40K was recorded in soil treated with FA at 40 t ha-1. The radioactivity due to addition of FA was subjected to dilution effect in soil. However, these marginal variations remained within the safe limit (Mittra et al. 2005).

2.0 Materials and method

2.1 Chemicals

Reagent grade barium chloride salt (AR) was purchased from Merck chemicals. Ultra-pure water produced by Milli RO-milli Q system was used throughout the synthesis process.

2.2 Sample and sampling technique

Two samples of AMD were collected randomly at different locations from West Rand Uranium mine situated in Gauteng Province in the Federal Republic of South Africa. The samples were stored in a plastic container and store in a refrigerator regulated at 4°C.

All chemicals used include absolute alcohol, barium chloride which are reagent grade merck chemicals and used without further treatment or purification.

2.3 Method

About 100 mL of acid mine drainage (AMD) was measured into a 500 mL beaker and agitated with a magnetic stirrer at 350 rpm speed. 30 mL of 1 M barium chloride

solution was added to the AMD in a drop wise manner which results in the formation of white precipitates. The precipitate formed from the addition of barium chloride to the AMD was constantly agitated for a contact time of 30 minutes in order to achieve homogeneity. The precipitate mixture was filtered off, washed with 100 mL of ultra-pure water thrice and dried in a regulated oven at a temperature of 80 °C for 3 hours. The dried precipitated was grounded gently by agate mortar before characterization.

$$BaCl_2 \text{ (aq)} + SO_4^{2-} \text{ (aq)} \longrightarrow BaSO_4 \text{ (s)} + 2Cl^- \text{(aq)}$$

2.4 Characterization
2.4.1 X-ray diffraction

The chemical composition of the AMD was determined with Variance Radial Inductively Coupled Plasma Optical Emission Spectroscopy (ICP-OES). The analysis of AMD with Dionex ion chromatography DX 4000i was used to determine the concentration of anions present in the AMD. The mineral phases present in the dried synthesized precipitate was identified by X-ray diffraction (XRD) analysis which was conducted on an Bruker axis D8 Advance X-ray powder diffractometer under CuKα radiation (λ = 1.5418 Å). The operation voltage and current at 40 KV and 40 mA, and the 2θ range from 10 to 80° in steps of 0.04° with a count time of 2 s. The average crystallite size of the precipitate was estimated automatically from corresponding XRD data (using X-ray broadening technique using the scherers formula). The morphology of the barium sulphate crystal was observed by scanning electron microscope (SEM) with accelerating voltage of 20 kV. Dried sample of $BaSO_4$ was placed on the coated carbon grid and allowed to dry at room temperature before the SEM analysis was conducted using a HITACHI S-4700 electron microscope. The elemental composition was identified using EDS spectrum that is recorded with the SEM instrument. The barium sulphate was prepared by the putting small amount of the particles in sample bottles containing 5ml absolute alcohol and sonicated for 10 minutes to obtain good particle dispersal on the copper grid and allowed to dry at room temperature. The morphology and particle size of the $BaSO_4$ was examined by Phillip Technei-F20 super-twain transmission electron microscopy (TEM) and the crystallinity of the crystals was conducted at an accelerating voltage of 200 kV. Fourier transform infrared (FTIR) analysis was conducted on the barium sulphate crystal to identify the functional groups present in the sample. The barium sulphate crystal was scanned within the range of 400 to 4000 cm-1. The Perkin Elmer FTIR spectrometer was used for recording the IR spectra crystal sample. The instrument was calibrated the spectra of a standard polystyrene film at room temperature. The barium sulphate crystal was prepared in pellet form before subjecting it to FTIR analysis and the spectra was recorded. Surface areas (BET area) of the $BaSO_4$ precipitates obtained from AMD was measured at a temperature of 77.35K using nitrogen adsorption method with a Quantachrome NOVA 2000 surface analyzer. Before the surface area analysis, the samples were prepared by washing the particles with acetone and drying them at 120°C for 5-8 hours under the flow of nitrogen.

3.0 Results and Discussion
3.1 Analysis of AMD

The AMD samples collected from two mining sites were analysed using ICP-OES for the elemental composition and IC for the anion composition is presented in Table 1. The elemental analysis shows that the concentrations of barium in the 2 samples were very small while that of Fe, Ca, Mg and Mn. However, the anion analysis of the 2 samples showed that the concentration of Cl was higher than that of NO_3 but sulphate was predominant species from both sources. RUD sample was the suitable AMD used for synthesis of barium sulphate because of its high concentration (4959.86 ± 58.50 mg/g).

Table 1. Analysis of cations and anions present in two AMD samples n = 3, RUD Rand Uranium Decant, RUS8 = Rand Uranium Shaft 8.

Sample	RUS8 (mg/L)	RUD (mg/L)
Al	1.74 ± 0.75	ND
Ba	0.014 ± 0.01	0.06 ± 0.03
Ca	395.68 ± 42.90	590.24 ± 31.90
Fe	296.73 ± 40.32	ND
Mg	140.11 ± 14.69	189.89 ± 10.42
Mn	70.69 ± 8.42	68.82 ± 4.36
Cl	49.94 ± 0.17	62.84 ± 1.16
NO_3	17.68 ± 0.64	56.41 ± 0.48
SO_4	2562 ± 615	4959.86 ± 58.50

3.2 Characterization

Figure 1 presents the X-ray diffraction patterns of the reagent grade and synthesized barium sulphate precipitates obtained from the AMD. The X-ray diffraction patterns of the crystallite showed some spectral peaks of barite mineral phase with reflection angles of 2θ indexed at 22.8°, 25.8°, 26.8°, 28.7°, 31.5°, 32.8°, and 42.9° which corresponds to (101), (111), (021), (210), (121), (211), (002), and (212) lattice plane of pure orthorhombic crystalline barium sulphate. The spectrum of the barite crystals contained all the major peaks referring to JCPDS file No. 24-1035 which is in good agreement with the results reported in the literature (Zhao *et al*, 2007; Romero-Ibarra *et al*. 2010; Sun *et al*. 2013; Wang *et al*. 2005; Wu *et al*, 2013). The mineral phase of the crystal precipitate was barite.
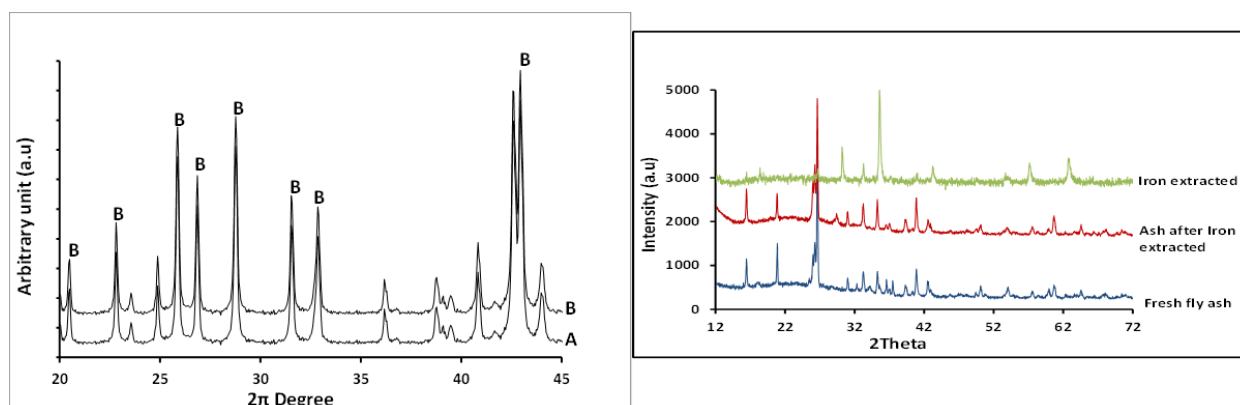
Figure 1. Powdered XRD pattern of fresh fly ash from Kriel thermal power station.

Figure 2 reveals the SEM images of reagent grade (A) and synthesized (B) barium sulphate ($BaSO_4.2H_2O$) and when viewed under the SEM revealed a star-like image with 8 petals lamellar. The SEM image was taken at a magnification of 30, 000 kv and the crystal size distribution of the barite in Figure 4 gave an average particle size diameter of 0.03 μm. The Energy-dispersive X-ray spectroscopy (EDS) spectral analysis of the barium sulphate crystal in Figure 2b revealed the spectra of elements such as Ba, S and O.
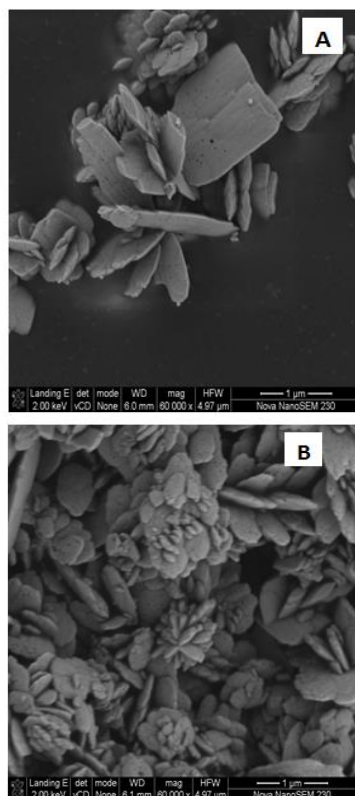
Figure 2. SEM microgram of reagent grade (A) and synthesized (B) of BaSO₄ precipitated from AMD.

Figure 3 presents the EDS elemental composition (a) and crystal size distribution (b) of the precipitated obtained from the AMD using barium chloride. The analysis showed that the precipitate was composed of C (10%), O (28%), S (9%) and Ba (54%). The presence of carbon in the precipitate can be attributed to the carbon coat used to hold the sample on the grid.
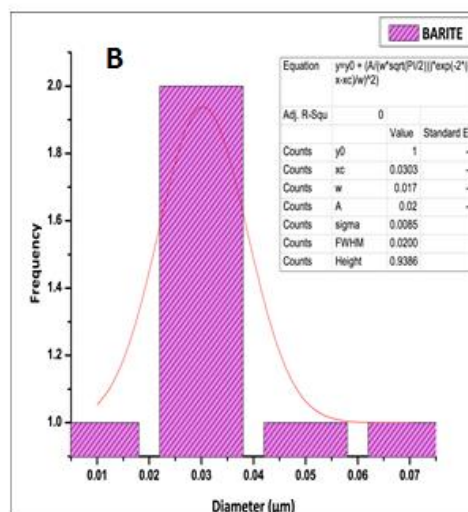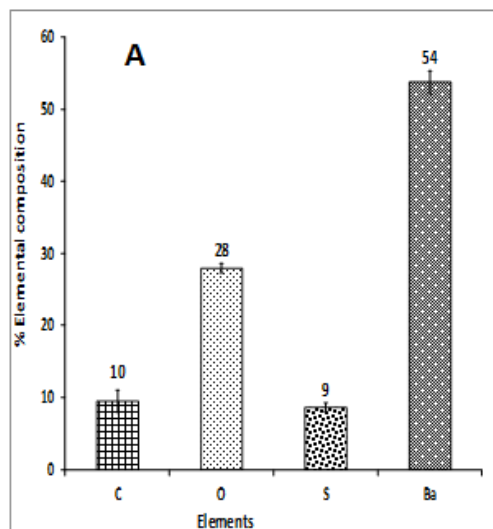
Figure 3. EDS elemental analysis (A) and crystal size distribution (b) of barium sulphate precipitated from AMD using barium chloride solution, n = 3.

Figure 4 presents the shape of the single-crystal of HRTEM image (a) and SAED (b) pattern of barium sulphate crystal precipitated from AMD using barium chloride. The shape of the $BaSO_4$ crystal is a 10 petal-like lamella structure with some snow-flakes and agglomeration at the top of the image. The particle size of the barium sulphate crystal was measured to obtain an average size diameter of 14 nm using image J software. The selected area electron diffraction (SAED) pattern of the barium sulphate crystal was recorded by focusing the electron beam at the brim of the sphere. The result shows the precipitate to be polycrystalline in nature because of the scattered white particle spots around the diffraction ring.
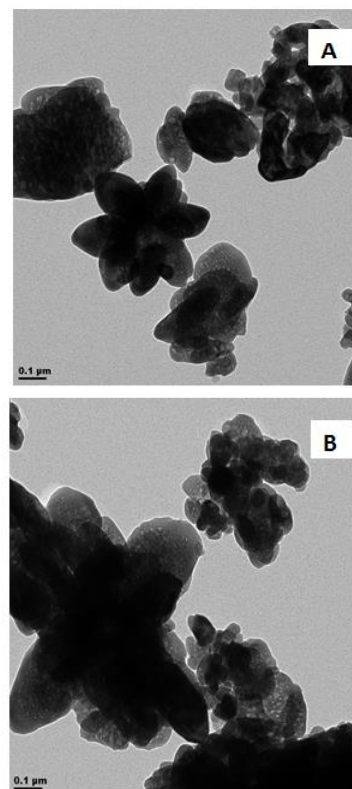
Figure 4. HRTEM microgram (A) and SAED (B) of barium sulphate crystals precipitated from AMD using barium chloride solution.
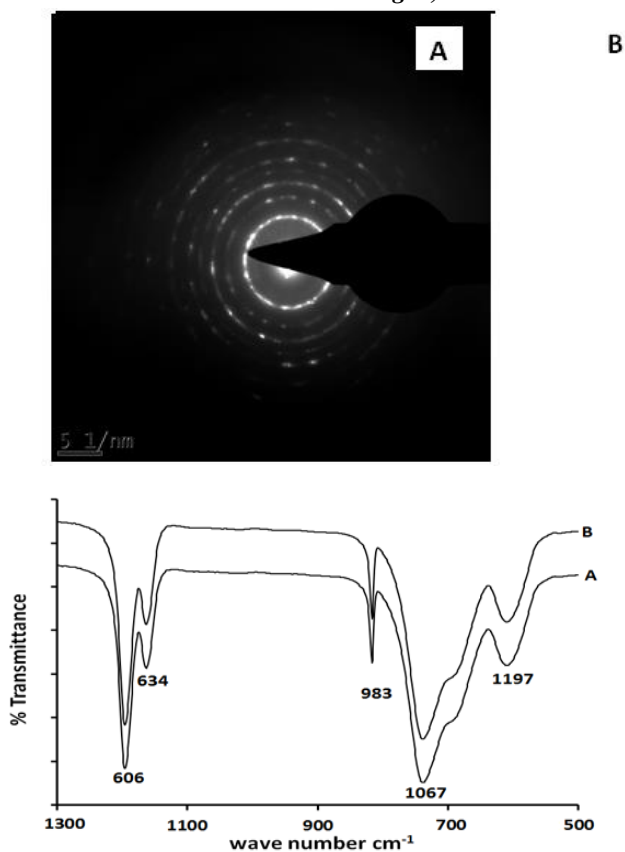
Figure 5. FTIR analysis of reagent grade (A) and synthesized barium sulphate crystals precipitated from AMD.
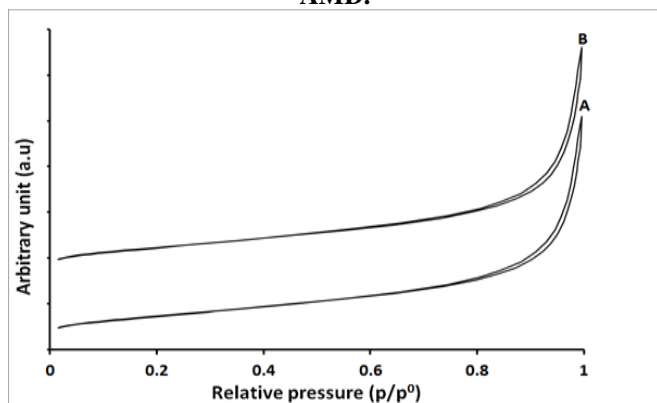
Figure 6. Nitrogen adsorption isotherm of reagent grade (A) and synthesized (B) barium sulphate precipitated from AMD solution

The FTIR absorption spectra analysis of barium sulphate crystal precipitate is presented in Figure 5a and the crystal was scanned between 400 and 1600 cm^{-1}. The observed FTIR absorption spectra of the barite crystal in Figure 6.4 showed absorption peaks at 606, 634, 982, 1060 and 1191 cm^{-1}. The absorption bands at 1060-1191 cm^{-1} are assigned to S-O stretching of inorganic sulphate while the peak at 984 cm^{-1} was assigned to the symmetrical vibration of sulphate. The absorption peaks at 606-634 cm^{-1} are assigned to bending vibrations of inorganic sulphate (Sun *et al*., 2013; Wu *et al*., 2013). The nitrogen adsorption-desorption isotherms of barium sulphate precipitated from AMD using barium chloride is presented in Figure 5b. The BET surface area of the crystal precipitates obtained in this study was 7.7 m^2/g and it exhibited poor porosity properties. The absorption isotherm of the barite sample is classified to be Type II which

is characteristic of mesoporous materials based on IUPAC classifications and the absorption-adsorption hysteresis loop is classified as H3 (Sing et al., 1985). The BET surface area of barium sulphate crystal precipitates obtained in this study was lower than some reported in the literature (Li and Yuan, 2006e) which was 2.3 m^2/g and 6.7 m^2/g for lamellar and agglomerated tubular barium sulphate respectively (Chen and Shen, 2010; Nagaraja *et al*., 2007) and higher than some found in the literature.

4.0 Conclusion

In summary, barium sulphate nanoparticle synthesized from acid mine drainage (AMD) by precipitation using barium. The use of barium ions have been reported to be very effective for the removal of sulphate ions in acid mine water and waste chemical solutions. The XRD analysis of the precipitate was identified as barite which is a mineral phase of pure barium sulphate. The diffraction analysis revealed that the particles of the precipitate are orthorhombic structure of barium sulphate. The morphology of the precipitate was identified with SEM as a star-like petal structure with 8 lamellar and the EDS spectral analysis confirmed that the presence of Ba, S and O elements on the surface of the precipitate. The HRTEM analysis of the particles of the precipitate showed a star-like petal lamellar structure of BaSO$_4$ with average particle size of 14 nm. FTIR study revealed the presence of sulphate group in the synthesized nanoparticles. The BET surface area of the precipitate was 7.7 m^2/g. In conclusion, the use of sulphate rich acid mine water as a substitute to the commercial reagent grade sulphate chemical was successful in the synthesis of barium sulphate nanoparticle.

References

1. Chen, Q., and Shen, X. (2010). Formation of mesoporous BaSO4microspheres with a larger pore size via Ostwald ripening at room temperature. CRYSTAL GROWTH & DESIGN,10(9), 3838-3842.

2. Sun, Y., Zhang, F., Wu, D., and Zhu, H. (2013). Roles of polyacrylate dispersant in thesynthesis of well-dispersed BaSO4 nanoparticles by simple precipitation.Particuology.

3. Wu,H.,Wang, C.,Zeng, C., and Zhang, L. (2013). Preparation of Barium Sulfate Nanoparticles in an Interdigital Channel Configuration Micromixer SIMM-V2. Industrial & Engineering Chemistry Research.

4.Zhang, M., Zhang, B., Li, X., Yin, Z., and Guo, X. (2011b). Synthesis and surface properties of submicron barium sulate particles. Applied Surface Science, 258(1), 24-29.

5. Claudia Telles Benatti, Celia Regina Granhen Tavares and Ervim Lenzi, (2009). Journal Environmental management, Vol 90, issue 1, January, Pages 504-511.

6. Wang, F., Xu, G., Zhang, Z., and Xin, X. (2005). Morphology control of barium sulfate by PEO-PPO-PEO as crystal growth modifier. Colloids and Surfaces A: Physicochemical and Engineering Aspects, 259(1), 151-154.

7. Ming XU, Haijun ZHANG, Changqing LIU, Yi RU, Guosheng LI, Yijun CAO (2017). A comparison of removal of unburned carbon from coal fly ash using a traditional flotation cell and a new flotation column. Physicochem. Probl. Miner. Process. 53(1), 2017, 628−643.

8. James C. Howera, John G. Groppoa, Uschi M. Grahama, Colin R. Wardb, Irena J. Kostovac, Mercedes M. Maroto-Valerd,g, Shifeng Daie (2017). Coal-derived unburned carbons in fly ash: A review. International Journal of Coal Geology, 179, 11–27.